Transient rift opening in response to multiple dike injections in the Manda Hararo rift (Afar, Ethiopia) imaged by time-dependent elastic inversion of interferometric synthetic aperture radar data

Raphael Grandin, A. Socquet, M.-P. Doin, E. Jacques, J.-B. de Chabalier, G. C. P. King

Transient rift opening in response to multiple dike injections in the Manda Hararo rift (Afar, Ethiopia) imaged by time-dependent elastic inversion of interferometric synthetic aperture radar data

R. Grandin,[1] A. Socquet,[1] M.-P. Doin,[2] E. Jacques,[1] J.-B. de Chabalier,[1,3] and G. C. P. King[1]

Received 14 August 2009; revised 13 April 2010; accepted 29 April 2010; published 9 September 2010.

[1] Interferometric synthetic aperture radar (InSAR) data spanning the time intervals separating thirteen dike intrusions in the Manda Hararo–Dabbahu rift (Afar, Ethiopia) from 2005 to 2009 show that transient deformation occurs in the inter-diking period. This deformation can be explained by the presence of seven inflating or deflating pressure sources. By combining the data acquired on four different InSAR tracks, through time-dependent elastic models, we are able to track these deformation modes with a time resolution smaller than 1 month. Sustained deflation of a deep magma reservoir at Dabbahu in the 6 months following the main rifting event of 2005, and slow decelerating post-eruptive re-inflation of two shallow magma reservoirs below Dabbahu and Gabho volcanoes, are monitored. A deflation signal of deep origin on the neighboring rift system is also detected, possibly caused by outflow of material from a preexisting reservoir into the deep plate boundary. In contrast, rapidly evolving deformation is observed at the center of the Manda Hararo rift segment. Transient deformation events are monitored in the weeks/months following the diking events, with pulses of localized rift opening after the dike intrusions, followed by an exponential-like decay of opening rate. This signal may be associated with the replenishment of the central magma reservoir involved in feeding the 2005–2009 dikes. Alternatively, the predominantly horizontal mode of deformation suggests an interaction between the response of the lithosphere to tectonic strain accumulation, and the process of hydraulic connectivity within the central magma plumbing system.

Citation: Grandin, R., A. Socquet, M.-P. Doin, E. Jacques, J.-B. de Chabalier, and G. C. P. King (2010), Transient rift opening in response to multiple dike injections in the Manda Hararo rift (Afar, Ethiopia) imaged by time-dependent elastic inversion of interferometric synthetic aperture radar data, *J. Geophys. Res.*, *115*, B09403, doi:10.1029/2009JB006883.

1. Introduction

[2] At mid-ocean ridges, the elastic strain continuously accumulated by plate divergence is relieved during rifting episodes that affect individual magmatic segments, and are separated by periods of quiescence lasting for several hundred years. Rifting episodes can last up to a few years, and consist of a succession of dike intrusions separated by weeks/months of reduced activity. Focused magma supply in the middle of the magmatic segment provides the material necessary for this crustal accretion process [e.g., *Macdonald*, 1982; *Smith and Cann*, 1999]. Normal faulting also plays a role in accommodating crustal extension, but the largely aseismic budget of mid-ocean ridges suggests that dike intrusions are more efficient in relieving tensile tectonic stress [*Solomon et al.*, 1988]. During a discrete diking event, magma is expelled from the central reservoir within a few hours, implying a fast pressure drop of the magma source [e.g., *Einarsson and Brandsdóttir*, 1980; *Björnsson*, 1985]. Replenishment of the reservoir is thus required to reach again the critical pressure level necessary for nucleating subsequent dike intrusions [e.g., *Buck et al.*, 2006]. Yet, although an interaction between magmatic and tectonic processes is suspected, the nature of the mechanism of repressurization is still debated.

[3] Surface deformation occurring during the inter-diking period may provide insights into the location, geometry and behavior of the central magma reservoir. A sequence of repeated dike intrusions is currently taking place in the Manda Hararo rift (Afar, Ethiopia) since September 2005 (Figure 1) [*Wright et al.*, 2006; *Ayele et al.*, 2007; *Grandin*

[1]Institut de Physique du Globe de Paris, Laboratoire de Tectonique et Mécanique de la Lithosphère, Paris, France.
[2]Laboratoire de Géologie, École Normale Supérieure, Paris, France.
[3]Observatoire Volcanologique et Sismologique de Guadeloupe, Gourbeyre, Guadeloupe, France.

0148-0227/10/2009JB006883

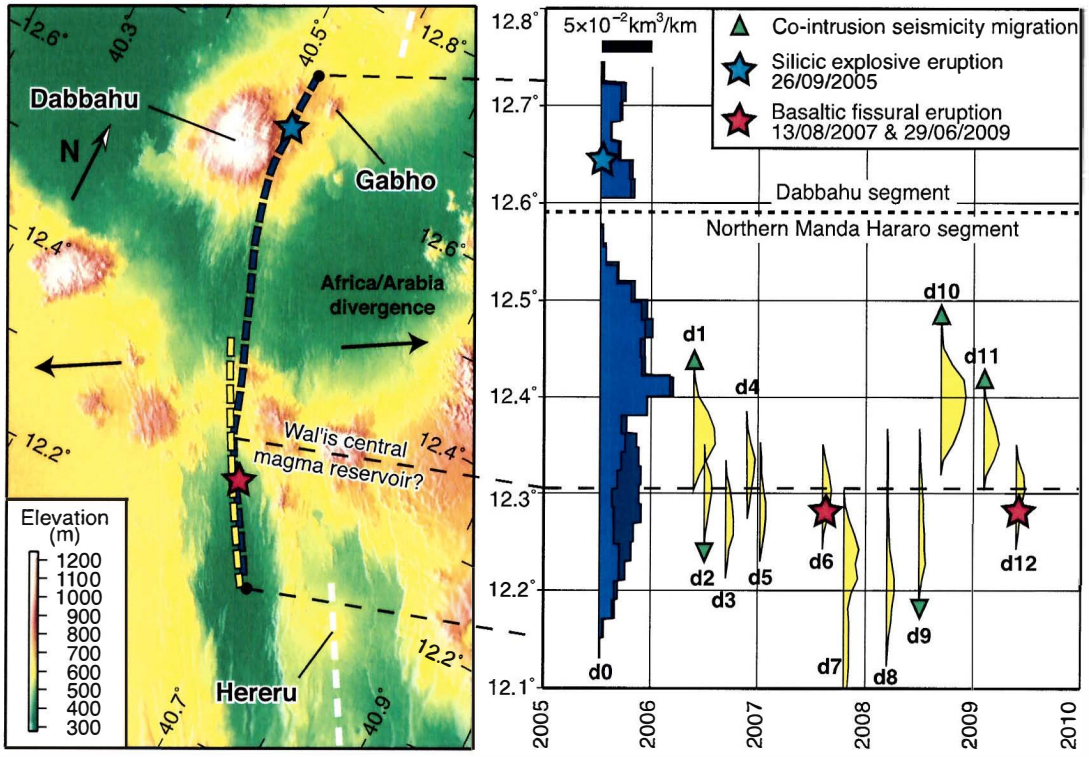

Figure 1. (left) Digital elevation model (DEM) of the Manda Hararo–Dabbahu rift. Thick dashed lines indicate the location of dike intrusions (blue, September 2005 mega-dike; yellow, 2006–2009 dikes). White dashed lines show the location of neighboring rift systems of Alayta (to the north) and Southern Manda Hararo (to the south). (right) Distribution of dike intrusions as a function of time and latitude, using the results of *Grandin et al.* [2009] for September 2005 mega-dike (d0, blue) and *Grandin et al.* [2010] for other dikes (yellow, d1–d12). Thickness of the colored curves indicates dike volume per unit distance along the dike (for instance, dike d10 has an average thickness of ~2 × 10^{-2} km^3/km integrated along its depth, and a length of ~10 km, yielding a volume of ~0.2 km^3). For the September 2005 rifting event, the light blue model is for no central magma reservoir deflation coeval to dike intrusion; the dark blue model includes hypothetic magma reservoir deflation at 10 km depth (see *Grandin et al.* [2009] for details). Green triangles show the direction of the migration of seismicity coeval to dike injection (using the results of *Keir et al.* [2009] for d1 and d2 and E. Jacques (personal communication, 2010) for d9, d10 and d11). Stars indicate eruptions. Horizontal dashed line indicates the approximate location of the inferred "Wal'is" central magma reservoir at 12.30°N.

et al., 2009]. This rifting episode, which occurs on a subaerial proto-mid-ocean ridge segment, represents an invaluable opportunity for monitoring processes of crustal accretion using high-resolution geodetic data. The main dike intrusion event of 2005 consisted of a 4 m-thick, 65 km-long, 8 km-high mega-dike with a volume of ~1–2 km^3 [*Wright et al.*, 2006; *Ayele et al.*, 2007; *Grandin et al.*, 2009]. Coeval to the rifting event, neighboring magma reservoirs at Dabbahu (9 km depth) and Gabho (4 km depth) experienced severe deflation. However, volume loss at these volcanoes, only representing ~25% of the total volume of the mega-dike, is probably related to the moderate silicic eruption that simultaneously occurred on the eastern flank of Dabbahu volcano. Also, the source of the magma that fed the mega-dike could not be conclusively identified from available seismic and geodetic data [*Wright et al.*, 2006; *Ayele et al.*, 2007; *Grandin et al.*, 2009].

[4] A total of twelve smaller dike intrusions (~0.1–0.2 km^3) were detected from June 2006 to June 2009 in the southern part of Manda Hararo rift. Following *Grandin et al.* [2010], these rifting events are numbered from d1 to d12, with d0 referring to the mega-dike of September 2005. Geodetic and seismological evidence indicate that these dikes propagated from the central part of the rift segment at ~12.3°N, suggesting that they were fed by a so-far undetected mid-segment reservoir [*Ebinger et al.*, 2008; *Keir et al.*, 2009; *Hamling et al.*, 2009; *Grandin et al.*, 2010]. A clear subsidence signal induced by deflation of this inferred magma source was observed coeval to the two distant dike intrusions d7 and d10, of November 2007 and October 2008 respectively (Figure S1 in the auxiliary material).[1] This reservoir was probably also active during the other dike intrusions in the sequence, including the September 2005 mega-dike intrusion [*Grandin et al.*, 2009; *Ayele et al.*, 2009], although geodesy cannot detect unam-

[1]Auxiliary materials are available in the HTML. doi:10.1029/2009JB006883.

biguously the deformation signal associated with this deep reservoir deflation when it is masked by the signal caused by dike intrusion at shallower depth [*Grandin et al.*, 2010].

[5] In this paper, we study the continuous deformation taking place from 2005 to 2009 in the Manda Hararo–Dabbahu rift in the time intervals separating the dike injections. The dense temporal sampling of InSAR is exploited to monitor the evolution of magmatic activity with time. This aims at understanding the dynamics of relaxation/recharge processes during the magmato-tectonic cycle at the temporal and spatial scale of a rifting episode, and to explore the possible interaction between magma reservoirs in the Manda Hararo rift.

2. InSAR Data

[6] Interferometric synthetic aperture radar (InSAR) is a geodetic technique that measures the deformation of the Earth's surface occurring between two passes of a satellite [e.g., *Massonnet and Feigl*, 1998; *Rosen et al.*, 2000; *Simons and Rosen*, 2007]. Only the component of displacement in the line-of-sight (LOS) of the satellite can be detected. This direction is nearly vertical, with a look direction either from the west (ascending pass) or the east (descending pass). In the Afar region, coherence of InSAR is excellent, due to arid climate, so that InSAR can determine surface deformation velocity accurately (down to a few mm/month), with a spatial resolution as low as ~100 m [e.g., *Grandin et al.*, 2009]. Following the Manda Hararo–Dabbahu 2005 rifting event, repeated acquisitions were performed by Envisat satellite between September 2005 and July 2009. The raw data set consists of 111 C-band SAR acquisitions (image-mode), acquired on two ascending tracks and two descending tracks (Figures S2, S3, and S4): 31 scenes for track 28 (ascending), 31 scenes for track 300 (ascending), 23 scenes for track 464 (descending), and 26 scenes for track 49 (descending). All tracks correspond to an incidence angle of ~20° with respect to the vertical, except track 464, which is more horizontal (~40°).

[7] Using this SAR data set, interferograms were processed with the ROI_PAC software [*Rosen et al.*, 2004]. Envisat state vectors calculated by ESA using DORIS orbits were used to subtract the orbital fringe pattern [*Zandbergen et al.*, 2002]. The topographic contribution to the interferometric phase was removed using a 90 m SRTM Digital Elevation Model (DEM) [*Farr and Kobrick*, 2001]. The unwrapping step was performed using the cut-tree algorithm [*Goldstein et al.*, 1988]. In the rift area where high fault scarps and creep on faults could induce important unwrapping errors, we prevent the phase from being unwrapped across the faults by introducing barriers that follow the faults trace [*Doubre and Peltzer*, 2007]. Prior to interpretation of InSAR data, interferograms were corrected jointly to reduce the amplitude of a topography-correlated perturbation induced by variations of the stratified tropostatic delay, which could otherwise be misinterpreted as a deformation signal in areas of prominent topography, such as volcanoes [e.g., *Beauducel et al.*, 2000; *Doin et al.*, 2009]. This was achieved by inverting for a residual planar orbital ramp (3 parameters per interferogram) and a phase/elevation ratio (1 parameter per interferogram), resolved on the parts of the interferograms that are not affected by ground deformation [e.g., *Cavalié et al.*, 2007]. Finally, InSAR images were downsampled at 8-looks (~150 m resolution).

[8] In order to monitor deformation in the Manda Hararo–Dabbahu rift, we have computed a total of 235 interferograms (Figure S2 and S3). All interferometric pairs with a temporal baseline of 35 days (the repeat time of Envisat acquisitions) and a perpendicular baseline less than 500 m (a limit above which the unwrapping errors caused by inaccuracies in the DEM become predominant) were processed. An effort was made to process the maximum number of interferograms with a small temporal baseline, and, for each track, to connect all SAR acquisitions by a network of InSAR images. Pairs with a temporal baseline greater than 35 days were also processed if their perpendicular baseline was less than 300 m, or if they were necessary to connect a "distant" scene to the interferometric network. This way, a series of differences and sums between well-chosen interferograms allows one to determine the deformation with a maximum resolution in time of 35 days [e.g., *Lundgren et al.*, 2001; *Berardino et al.*, 2002; *Doubre and Peltzer*, 2007].

3. Deformation Styles in the Inter-diking Period

3.1. Preliminary Elastic Inversion

[9] The InSAR data set described in section 2 reveals that from September 2005 to July 2009, apart from discrete dike injections that have affected the axis of the Manda Hararo–Dabbahu rift [*Wright et al.*, 2006; *Grandin et al.*, 2009; *Hamling et al.*, 2009; *Grandin et al.*, 2010], significant deformation has also occurred during inter-diking periods. Using a classical pixel-by-pixel inversion [*Schmidt and Bürgmann*, 2003], we were able to retrieve the incremental LOS deformation between successive SAR acquisitions, independently for each track (see Animation S1 in the auxiliary material). A visual analysis of the resulting time series shows that deformation is time dependent, and that a finite number of sources of deformation can be identified. The aim of this paper is to follow their behavior with time. For this purpose, their respective contributions must be determined using a model that accounts for the observed LOS displacements at any time. We may then deduce the evolution of activity of each source by linking together all available InSAR images on the four different tracks, into a single, time-dependent inversion. However, this requires to solve a strongly non-linear inverse problem, a task that cannot be performed in a single step. Nevertheless, the problem becomes linear as soon as the nature and the geometrical parameters of the sources of deformation is known. This motivated our strategy of, first, performing a non-linear inversion of InSAR data spanning different time intervals in order to identify the sources of deformation, and, in a second step, solving a linear inverse problem that enables us to follow the temporal behavior of activity of these sources, by using the whole InSAR data set. Details of the inversion strategy are given in Appendix B.

[10] As a first step, we determine the smallest number of sources that explain the deformational signal detected by InSAR throughout the inter-diking period (Table 1). This is done by modeling deformation using sources embedded in an elastic half-space. The sources are either rectangular dislocations [*Okada*, 1985] or spherical pressure sources

Table 1. Geometric Features of the Dislocation Elements and Mogi Sources Used in the Elastic Time Series Inversion[a]

Element	Longitude[b] (°N)	Latitude[b] (°N)	Depth[b] (km)	Width[c] (km)	Length (km)	Strike (°N)	Dip (°N)
D1	40.477	12.575	8.8	1.0	1.0	0.0	0.0
D2	40.469	12.600	4.9	1.0	1.0	0.0	0.0
G	40.540	12.681	3.8	1.0	1.0	0.0	0.0
W1	40.629	12.306	4.0	6.0	8.0	150.0	90.0
W2	40.614	12.302	4.0	ND	ND	ND	ND
W3	40.614	12.302	25.0	ND	ND	ND	ND
H	40.850	12.099	17.0	ND	ND	ND	ND

[a]D1, D2, G, and W1 are dislocation elements, and W2, W3, and H are Mogi sources. ND, not defined.
[b]Location of the middle of the top of the dislocation.
[c]Width of dislocation along dip.

[*Mogi*, 1958]. A non-linear inversion scheme is applied to deduce the geometrical and kinematic characteristics of these sources using InSAR data [*Tarantola and Valette*, 1982]. The inversion procedure is described by *Grandin et al.* [2009]. Prior to the inversion, an adapted down-sampling scheme is applied to each interferogram in order to keep the problem computationally tractable [e.g., *Simons et al.*, 2002; *Jónsson et al.*, 2002]. Following *Grandin et al.* [2009], a greater density of data points is kept in the vicinity of the inferred sources of deformation, whereas distant regions in the interferograms are more severely down-sampled (Figure S4). No further weighting of data points is performed. In order to assess the consistency of the deformation patterns in time, a large number of elastic inversions were performed for several time intervals spanning the rifting episode (Figures S5 and S6). For each inversion, two InSAR images acquired on ascending and descending tracks were used, with as much overlapping in time as possible (Table S1). This allows one to distinguish between vertical and horizontal components of deformation, and hence improve the inversion [e.g., *Fialko et al.*, 2001b].

[11] As an example of the result of the inversion of InSAR data during an inter-diking interval, we show two interferograms in Figure 2, which we compare with the synthetic deformation deduced from the inversion. The interferograms span a period of time following the September 2005 mega-dike, between early December 2005 and late May 2006 (175 days, 98% overlap in time). Cross-sections in the observed and modeled deformation fields are shown in Figure 3, with elevation and model setting for reference. Each source of deformation is described in detail in section 3.2.

3.2. Description of the Sources of Deformation

[12] In the Dabbahu–Gabho area, at least three sets of concentric fringes are observed on both ascending and descending interferograms during various periods from 2005 to 2009 (Figure 2). There, deformation is predominantly vertical, and is best explained by three distinct point sources modeled as horizontal 1 km^2 square dislocations at depths of 8.8 km (source D1), 4.9 km (source D2) and 3.8 km (source G) (Figure 3). They are interpreted as deflating or inflating sill-like pressure sources at depth. Sources D1 and G may reflect the renewed activity of the magma reservoirs that were observed to have deflated below Dabbahu and Gabho coeval to September 2005 mega-dike intrusion [*Wright et al.*, 2006; *Grandin et al.*, 2009].

[13] Similarly, a broad subsidence signal is detected in the vicinity of Hereru volcano, on the neighboring "Manda Hararo Volcanic Range" [*Tazieff et al.*, 1972; *Barberi et al.*, 1972], ~20 km to the ESE of the southern tip of the September 2005 mega-dike. The radius of the nearly concentric fringes (~25 km) suggests that it may be caused by a deep-seated deflating source, or distributed deformation affecting a shallower region of the lithosphere (Figure 3). In the following, we model the concentric fringes in the Hereru area using a Mogi source lying at 17 km depth (source H).

[14] Along the Manda Hararo rift axis, to the south of Dabbahu volcano, numerous InSAR fringe discontinuities are observed in the months following the 2005 rifting event. They were mapped by *Grandin et al.* [2009], who interpreted them as motion on faults and/or fissures in the subsurface, as a result of post-rifting readjustments. The high degree of complexity of this short-wavelength deformation signal makes its interpretation difficult, and these features will not be discussed here. In the following, the region bounded by the faults and fissures located on each side of the rift axis is masked, and the subsidence associated with these faults is not taken into account. Instead, we focus our analysis on a smooth deformation signal in the center on the Manda Hararo rift, indicative of deep processes. This area is denominated "Wal'is area," following *Grandin et al.* [2009].

[15] Figure 4 shows the evolution of the LOS velocity field in the center of the Manda Hararo rift as a function of time, showing that deformation there is not stationary in time. Moreover, in contrast to the sources described at Dabbahu and Hereru, we observe a "butterfly" fringe pattern centered on the Manda Hararo rift at ~12.30°N, with significant differences in the fringe pattern for InSAR images acquired either on ascending or descending tracks (Figures 2 and 3). This feature is similar to what is observed during a dike intrusion [e.g., *Grandin et al.*, 2009], suggesting an important component of horizontal deformation, which cannot be explained by a simple pressure source at depth (e.g., Mogi, sill), but requires rift-perpendicular opening at depth.

[16] Furthermore, the fringe pattern is not stationary in space. In some time intervals (e.g., interval i in Figure 4), we observe a "bull's eye" fringe pattern, which is consistent with the presence of a pressure source at depth, in addition to the opening component. This source lies at the same location as the deflating magma reservoir observed by InSAR coeval to the rifting events of November 2007 and October 2008 (Figure S1), which presumably fed the dikes of the 2005–2009 rifting episode [*Hamling et al.*, 2009; *Grandin et al.*, 2010]. However, the radius of the area affected by uplift in the inter-diking periods appears to be broader than that caused by a source at 7–10 km depth (determined by *Hamling et al.* [2009] for the November 2007 deflation), and another deeper source must be invoked.

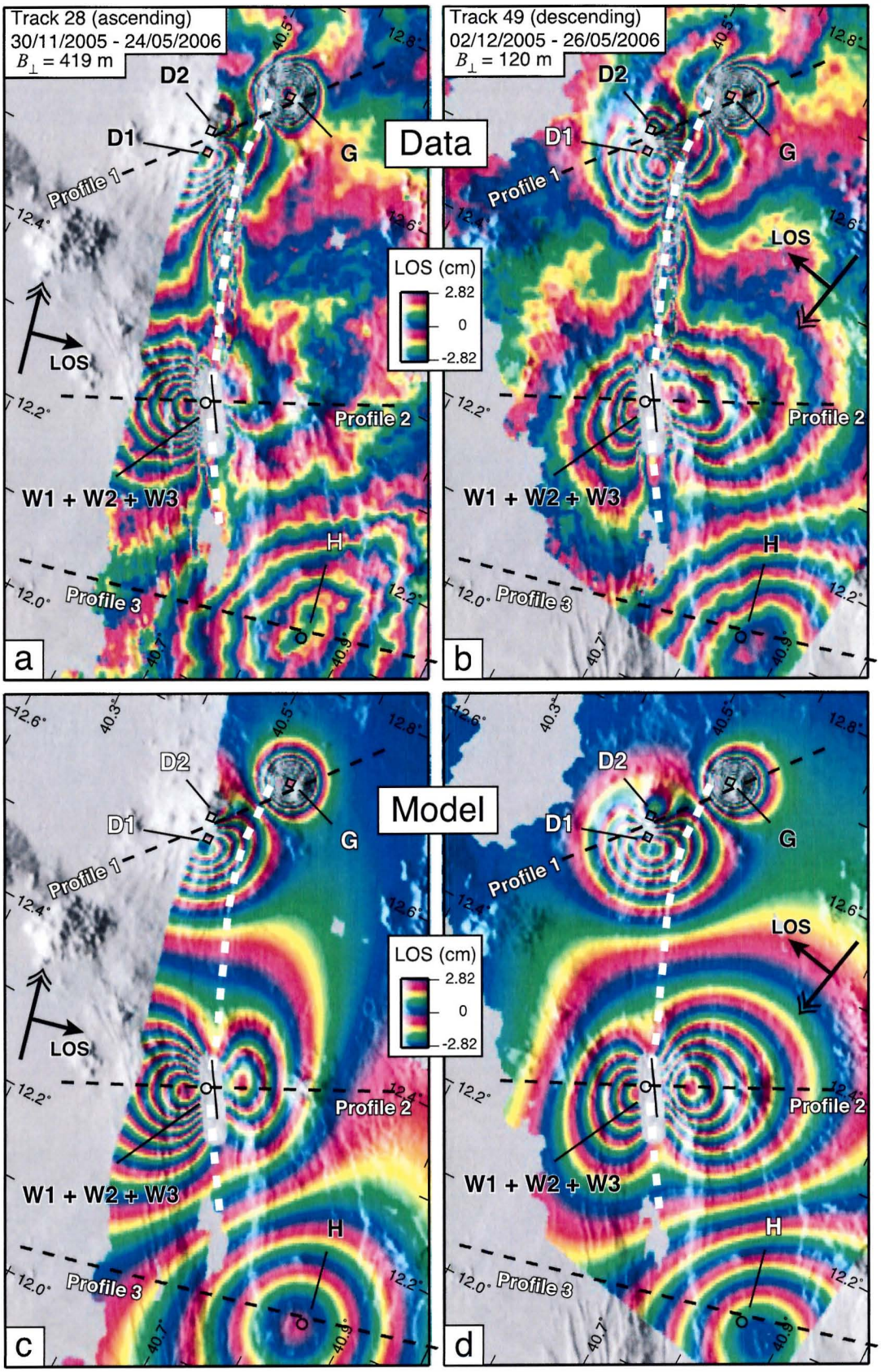
Track 28 (ascending)
30/11/2005 - 24/05/2006
$B_\perp$ = 419 m
Track 49 (descending)
02/12/2005 - 26/05/2006
$B_\perp$ = 120 m
Data
Model
D1
D2
G
H
Profile 1
Profile 2
Profile 3
LOS
LOS (cm)
2.82
0
-2.82
W1 + W2 + W3
a
b
c
d

Figure 2

A minimum of three sources of deformation are thus required to explain the complex fringe pattern in the Wal'is area (Figure 3): the bulk of the horizontal deformation can be reproduced with an 8 km long, vertical, inflating (tensile) dislocation, extending from 4 km to 10 km depth, striking parallel to the rift trend (source W1); localized uplift/subsidence can be modeled by the presence of two Mogi sources, located at 4 km (W2) and 25 km (W3) depths.

[17] The analysis carried out in this section was based on the inversion of InSAR data spanning various time intervals of the 2005–2009 Manda Hararo–Dabbahu rifting episode, taking advantage of the different look directions of the satellite to infer the nature and depth of the sources that induce the observed deformation. We have shown that seven sources are sufficient to explain the pattern of deformation observed at any time. However, a broad range of different sources would also fit the InSAR data reasonably well in most areas. For instance, depth estimates of point sources strongly trade-off with the source geometry, which is difficult to constrain solely based on geodetic data [e.g., *Dieterich and Decker*, 1975; *Fialko et al.*, 2001a; *Dzurisin*, 2006]. Figure S7 illustrates the trade-off in our inversions between source depth and volume change, and the almost equal ability of different types of pressure sources (e.g., Mogi or sill-like source) to explain the observed deformation. Possible modeling alternatives include: spherical versus ellipsoidal source, sill-like versus penny-shaped crack, extended source versus point source, tall dike versus short dike plus deep Mogi source. This should be kept in mind during the interpretation of the time-dependent inversions developed in section 4, especially for deep sources, which produce low-amplitude deformation spread over a large area at the surface. As a consequence, the solution of the inversion of InSAR data is non-unique, and uncertainties on model parameters are difficult to assess.

4. Time Series Inversion

4.1. Method

[18] Using the synthetic deformation produced by elastic modeling of the seven sources, the rate of deformation of each source is inverted as a function of time. The short recurrence time between discrete dike injections in 2006–2009 (from 1 to 9 months) impedes a continuous monitoring of the deformation taking place at the center of Manda Hararo rift. Instead, "source time functions" (STFs) are calculated piecewise on inter-dike intervals separately, using the 96 downsampled interferograms that are not affected by co-diking deformation (Figures S2 and S3). Projection of the 3D deformation of the surface deduced from elastic modeling is performed according to the LOS vector of each track. The resulting elastic Green's functions act as the bridge between the intensity of each source of deformation and the LOS deformation actually captured by a given interferogram. By combination of all InSAR images acquired on the four tracks, it becomes possible to construct time series of the activity of each source of deformation during each independent inter-dike period.

[19] In order to stabilize the inversion, a temporal smoothing scheme is implemented (Figure S8). A single smoothing parameter controls the degree to which the rate of inflation/deflation of each source is permitted to change with time. The smoothest solution corresponds to a piecewise steady state signal, and the inversion can be tuned toward progressively non-steady (rougher) source time functions. Across each dike injection, inflation rates are not determined. The resulting temporal resolution is high (~ 10 days), thanks to the combination of InSAR data from different tracks. A non-negativity constraint is imposed on the sense of opening or closure of each dislocation at any time. This method is similar to that of *Pritchard and Simons* [2006], who also linked data from different InSAR tracks, as well as GPS data, to infer spatiotemporal variations of slip on the subduction interface of northern Chile, on timescales as short as 2 months. In Afar, the greater velocity of surface deformation and frequent SAR acquisitions allow us to extend the analysis to smaller time intervals, and to detect transient deformation events that occur during shorter inter-diking intervals. However, the amount of smoothing that we have chosen results in an effectively decreased time resolution, and sharp changes of inflation rates of the sources of deformation are spread over several weeks by the inversion. We estimate that this allows us to determine changes of inflation rate down to a resolution of 1 month.

4.2. Results

[20] In Figure 5, the result of the time series inversion is displayed. All sources show variations of their inflation or deflation rate throughout the 2005–2009 period. At Dabbahu, deflation is detected from October 2005, until May 2006 (D1). This transient deflation is superseded from January 2006 by inflation of a magma reservoir at a shallower depth (D2), and observed at least until mid-2009, with a decaying rate from mid-2007. In contrast, inflation of Gabho magma reservoir (G) is observed to accelerate from January 2006, and then to regularly decay until the end of 2007, when the reservoir does not produce detectable deformation anymore. None of the pressure sources in the Dabbahu area exhibit a clear change of deflation or inflation rate across any diking event. These results provide an explanation of the evolution of the vertical component of displacement at two sites above Dabbahu and Gabho volcanoes, where two continuous GPS receivers (GABH and DABB) were operated from early 2006 to early 2007 [see *Hamling et al.*, 2009, Figure 3].

Figure 2. (a and b) Deformation imaged by InSAR between early December 2005 and late May 2006. $B_{\perp}$: perpendicular baseline between master and slave images. (c and d) Synthetic deformation produced after elastic inversion. The heading direction of the satellite is shown by a double headed arrow, and line of sight (LOS) by a perpendicular black arrow. Increasingly negative range-change corresponds to increasing distance between the satellite and the ground. For instance, fringes at Hereru indicate that the ground is moving away from the satellite, whereas deformation at Gabho corresponds to motion toward the satellite. Location of the September 2005 dike is indicated by the white dashed line. D1, deep Dabbahu; D2, shallow Dabbahu; G, Gabho; H, Hereru; W1, Wal'is "dike"; W2, Wal'is shallow Mogi source (4 km); W3, Wal'is deep Mogi source (25 km). See Table 1 for details of the geometry of sources of deformation.

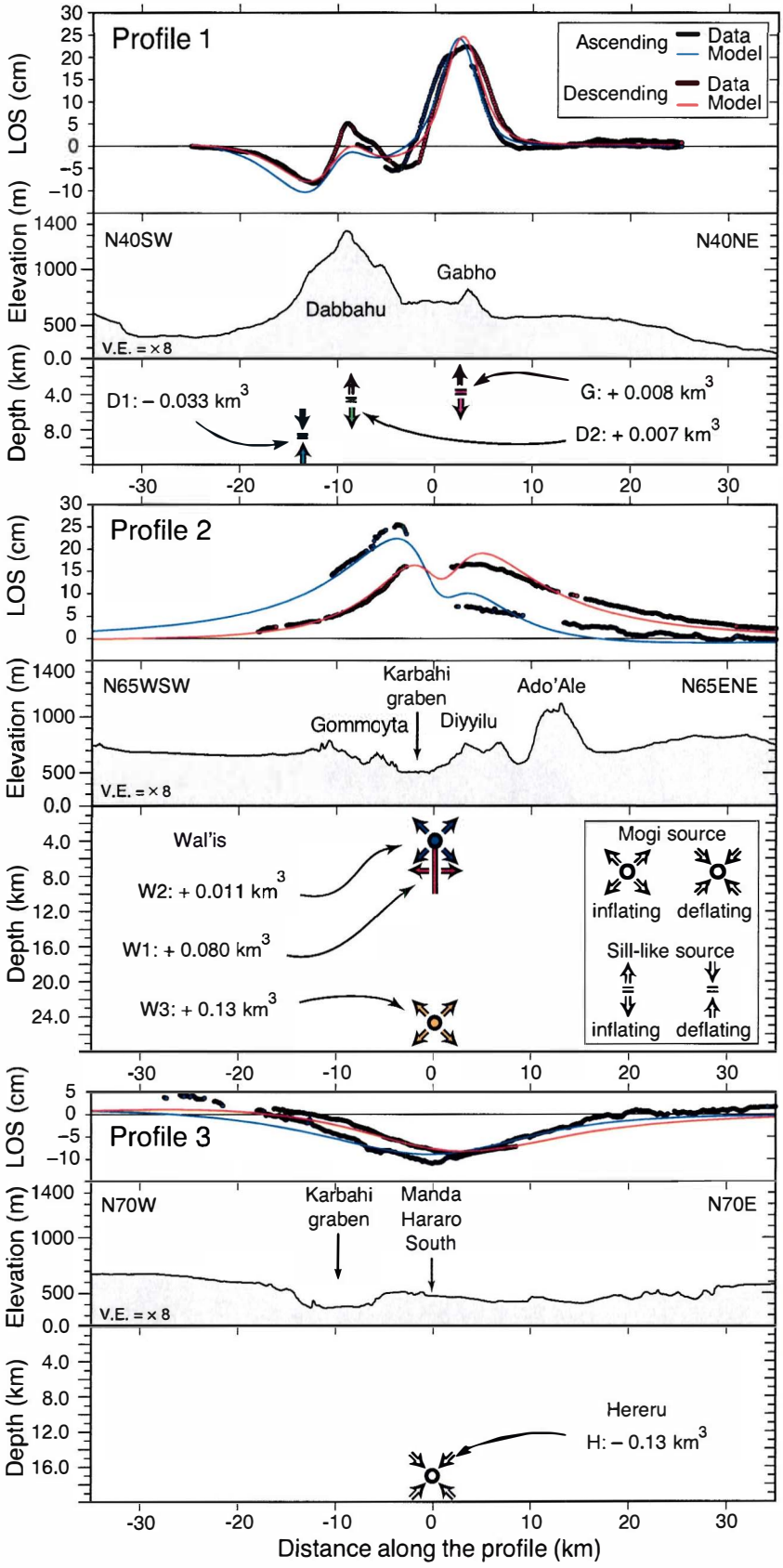
Profile 1
Ascending
Data
Model
Descending
Data
Model
LOS (cm)
Elevation (m)
N40SW
N40NE
Gabho
Dabbahu
V.E. = × 8
Depth (km)
D1: – 0.033 km3
G: + 0.008 km3
D2: + 0.007 km3
Profile 2
N65WSW
Karbahi graben
Ado'Ale
N65ENE
Gommoyta
Diyyilu
Wal'is
W2: + 0.011 km3
W1: + 0.080 km3
W3: + 0.13 km3
Mogi source
inflating
deflating
Sill-like source
inflating
deflating
Profile 3
N70W
Karbahi graben
Manda Hararo South
N70E
Hereru
H: – 0.13 km3
Distance along the profile (km)

Figure 3

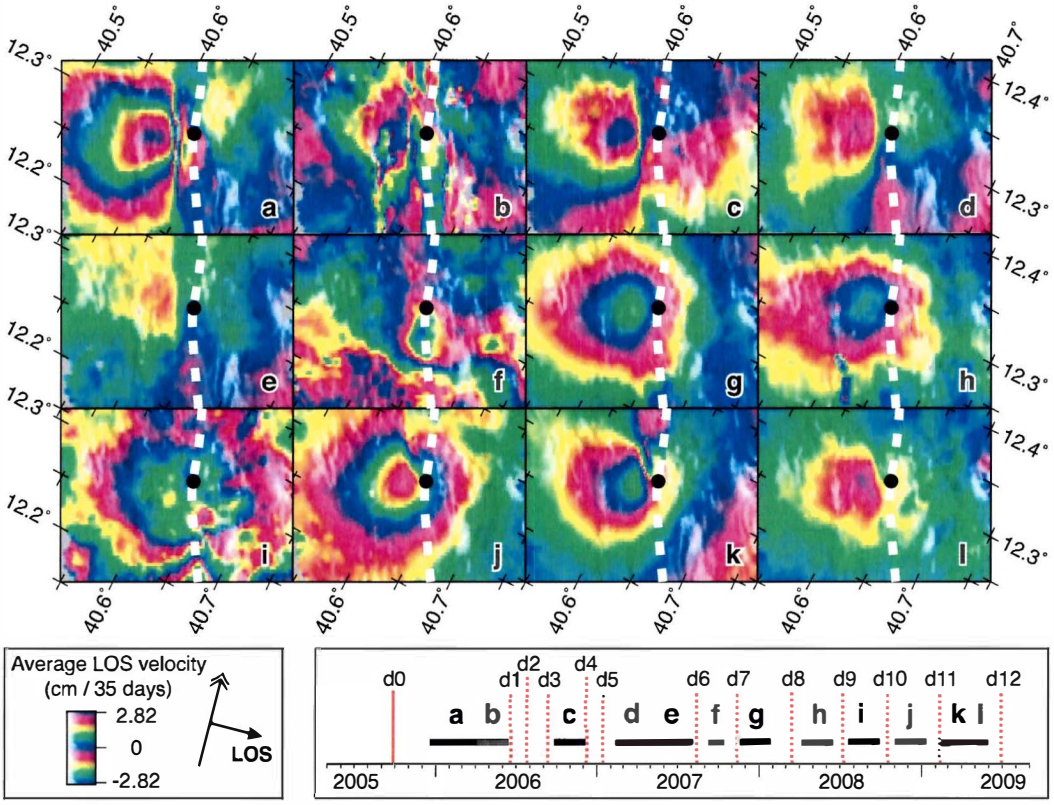

Figure 4. Average line-of-sight (LOS) displacement velocities in the Wal'is area for 12 time intervals. One fringe corresponds to a LOS displacement velocity of 2.82 cm per period of 35 days (the repeat time of Envisat acquisition). The convention of color scale is the same as in Figure 2. The fringes visible on the left correspond to motion toward the satellite. Time spanned by each interval is indicated in the bottom right. Interferograms from track 300 (ascending) were used to construct this time series. The black dot indicates the location of the inferred magma supply at depth (sources W2 and W3 in Figures 2 and 3). Subsidence at rift axis during interval f is interpreted to result from the deflation caused by post-diking cooling and freezing of dike d6 (August 2007), which emplaced at shallow depth (less than 5 km) and led to a fissural eruption [*Grandin et al.*, 2010].

[21] Deflation at Hereru (H) occurs at a nearly constant rate since October 2005, perhaps with a small decrease of deflation rate in mid-2007. Similarly, the deepest source at Wal'is (W3) inflates at a nearly constant rate from 2005 to 2009. Shorter-term variations of the rate of deflation of sources H and W3 are probably unreliable due to the great depth of the sources.

[22] The two sources located at shallow depths in the center of the Manda Hararo, in the Wal'is area (W1 and W2), show different patterns. For the dike-like source (W1), after a fast inflation period lasting for nearly 6 months after the intrusion of September 2005 mega-dike, opening strongly decelerates in the following years. In addition, we notice that, superimposed on this overall pattern of decreasing inflation rate, sharp increases of the inflation rate of W1 are detected after most diking events, followed by periods of progressively decreasing rate of inflation, lasting for months in the inter-diking intervals. This behavior is clear when the first time derivative of opening is plotted as a function of time (Figure 6). In contrast to other sources, a simple model of exponentially decreasing rate of inflation cannot explain this behavior. The Mogi component (W2) may show a similar evolution, but rapid changes of inflation rate are less systematic and more tenuous, and the STF weakly departs from steady state or exponentially decaying inflation.

4.3. Estimation of the Cumulative Volume Changes

[23] Using the results described above, the volumes involved in inflation or deflation of the above sources can be determined in the intervals covered by InSAR data. However, due to a lack of data, or to dike injections that mask the signal in the inter-diking period immediately before or after the dike intrusion, data coverage is not continuous in time. This produces gaps in the time series that prevent us from estimating the total volume change during the whole period.

Figure 3. Three cross sections showing (bottom) the location of the pressure sources, (middle) surface elevation, and (top) LOS displacement at the surface for the interferograms of Figure 2 (dots, data; continuous line, model). See Figure 2 for location of the profiles.

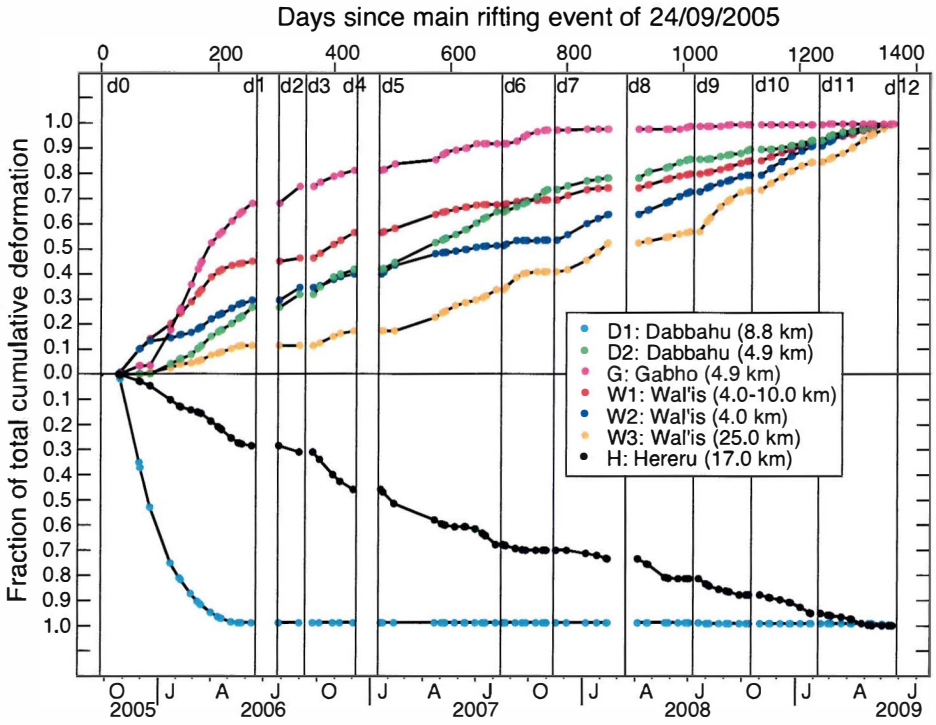

Figure 5. Source time functions (STFs) for the seven sources of deformation (color dots) deduced from inversion of inter-diking InSAR data, with preferred smoothing intensity (see text and Figure S8 for details). STFs are normalized to the total cumulative deformation between 2005 and 2009. The origin time is the date of the September 2005 mega-dike intrusion (d0); vertical lines indicate the dates of occurrence of rifting events in the Manda Hararo rift (d1 to d12). Data spanning the intervals that bracket a dike intrusion (vertical black lines) are discarded, and STFs are not constrained in these intervals.

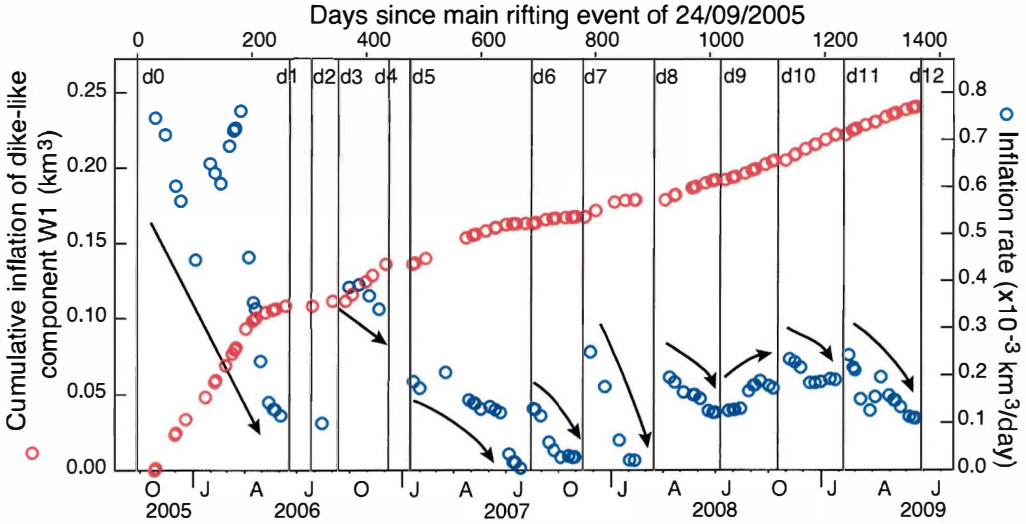

Figure 6. STF for dike-like source W1 at Wal'is (red circles, same as red dots in Figure 5) and inflation rate (first time derivative) computed in each interval spanning two successive points of the STF (blue circles). A sudden increase in inflation rate is observed after most rifting events, followed by a decrease in inflation rate in the following months (arrows).

Nevertheless, assuming that deformation is sufficiently regular in time, it is possible to extrapolate the time series deduced from the elastic inversion to intervals where no data is available. For this purpose, the above STFs are fitted with simple analytic functions of time (Figure 7).

[24] The STF for source W3 is found to be best described as a source inflating at constant rate. Sources H and D1, as well as W2, are modeled by an exponentially decaying rate of deflation or inflation. The optimal characteristic times of the exponentials are found to be of the order of several years at W2 and H (1878 days and 1222 days respectively), corresponding to a nearly steady state behavior. A much smaller characteristic time is found for D1 (73 days). STFs at D2 and G are fitted by the same functions, except that delays of 75 days and 100 days are introduced, respectively, prior to onset of activity. Optimal characteristic times are 991 days for D2, and 226 days for G. In contrast, the "dike" component of deformation at Wal'is (W1) seems to follow a succession of exponentials, with a characteristic time of 250 days, triggered by each successive dike intrusion (see Appendix C for details of the method of computation of the exponentials).

[25] Inflation of the dike-like source W1 dominates the budget of volume change at shallow depth in the Manda Hararo–Dabbahu rift, with a cumulative volume increase of +0.35 km^3 (Figure 7). Sources W2 and W3, which predominantly induce uplift at the rift axis, do not exhibit strong variations of activity, and seem to inflate at a nearly constant rate, reaching, by extrapolation, a cumulative volume of +0.08 km^3 and +0.9 km^3, respectively. This latter value may be compared to deflation of source H, which accounts for nearly −0.8 km^3. In contrast, volumes changes involved in the Dabbahu area are one order of magnitude smaller: −0.09 km^3 at D1, +0.05 km^3 at D2, and +0.017 km^3 at G.

5. Discussion

5.1. Assumption of Elasticity

[26] Prior to interpretation of these result, a major assumption of the modeling has to be clarified. Accordingly, deformation accumulating over periods of months to years is expected to depart from purely elastic. In particular, deformation interpreted as being caused by an elastic source located deeper than 10–15 km depth may be explained equally well by alternative models (e.g., distributed flow, visco-elastic relaxation). However, it has been shown that the linear theory of elasticity can reproduce the deformation of the surface of the Earth even at geologic timescales when the lithosphere is thought to deform inelastically, suggesting that the underlying processes governing the evolution of topography cannot always be constrained by data sets consisting of surface deformation measurements [e.g., *Armijo et al.* 1996]. Hence, the nature of the processes that cause transient deformation in the Manda Hararo area is not discussed in view of the InSAR fringe pattern alone. Instead, the focus of this study is to determine the "source time function" (STF) associated with each source, in an attempt to draw conclusions from this time-dependent behavior. In this view, the elastic theory is used to build Green's functions that can then be combined with the data to invert for the time variations of the intensity of each source of deformation. Yet, this does not necessarily mean that elastic behavior actually governs the deformation in the area during the inter-diking period.

[27] Another issue is the reliability of volume determinations. There exist various trade-offs between source depth, source geometry, and intensity of the source that allow the observed surface displacement to be fit by a variety of models (Figure S7). Thus, the values of inferred cumulative volumes presented in this paper should be regarded with caution, especially for the deeper sources. Nevertheless, we notice that the volume changes that we have determined during the long periods of slow deformation considered in this study, are systematically smaller than those deduced from short events of rapid mass movement, although the same type of geodetic data is used. For instance, volume balance is not satisfied at Gabho and Dabbahu, with a total deflation of nearly −0.5 km^3 in September 2005 [*Wright et al.*, 2006; *Grandin et al.*, 2009], and only +0.07 km^3 of re-inflation in the 2005–2009 period [this study]. Furthermore, the cumulative volume of all dike intrusions in the Manda Hararo–Dabbahu rift from June 2006 to June 2009 (~1.0 km^3 [*Grandin et al.*, 2010]) is not compensated by sufficient inflation of the shallow reservoirs at Wal'is in the inter-diking period (~0.4 km^3 [*this study*]). This is in keeping with the observation of *Hamling et al.* [2009], who noted that volume loss at Wal'is magma reservoir coeval to November 2007 dike intrusion is much smaller than dike inflation itself (−0.025 km^3 versus +0.15 km^3). Unless rapid cycles of inflation and deflation that were not captured properly by InSAR have occurred, these differences cannot be explained by inappropriate modeling if deformation is nearly elastic.

5.2. Deformation in the Dabbahu Area

[28] At Dabbahu, subsidence observed after the main rifting event seems to involve the same deep deflating source (source D1) as that identified during the September 2005 event (Figure 7) [*Wright et al.*, 2006; *Grandin et al.*, 2009]. This signal may reflect the slow discharge of the Dabbahu magma reservoir into the mega-dike that emplaced along the Manda Hararo rift and that came into contact with magma reservoirs that preexisted in the Dabbahu area in September 2005 [*Grandin et al.*, 2009; *Ayele et al.*, 2009]. The duration of the subsidence (a few months) may be controlled by a progressive freezing and closure of the connection between the deep Dabbahu magma reservoir and the mega-dike body. This may be confirmed by the decay of seismicity detected in the same period along the northern part of the Manda Hararo rift [*Ebinger et al.*, 2008], which may represent a proxy of the inflation rate of the mega-dike in this area.

[29] In contrast, decelerating inflation of shallow Dabbahu (D2) and Gabho (G) magma reservoirs is similar to that reported after volcanic eruptions for other volcanoes such as Grimsvötn (Iceland), Mauna Loa (Hawaii), Piton de la Fournaise (La Réunion), or Westdahl (Alaska) [e.g., *Delaney et al.*, 1990; *Lu et al.*, 2003; *Sturkell et al.*, 2003; *Lengliné et al.*, 2008]. It may reflect the partial repressurization of the magma reservoirs.

[30] Finally, we note that the inflation/deflation rates of pressure source in the Dabbahu area do not change abruptly prior or after any discrete dike emplacement in the

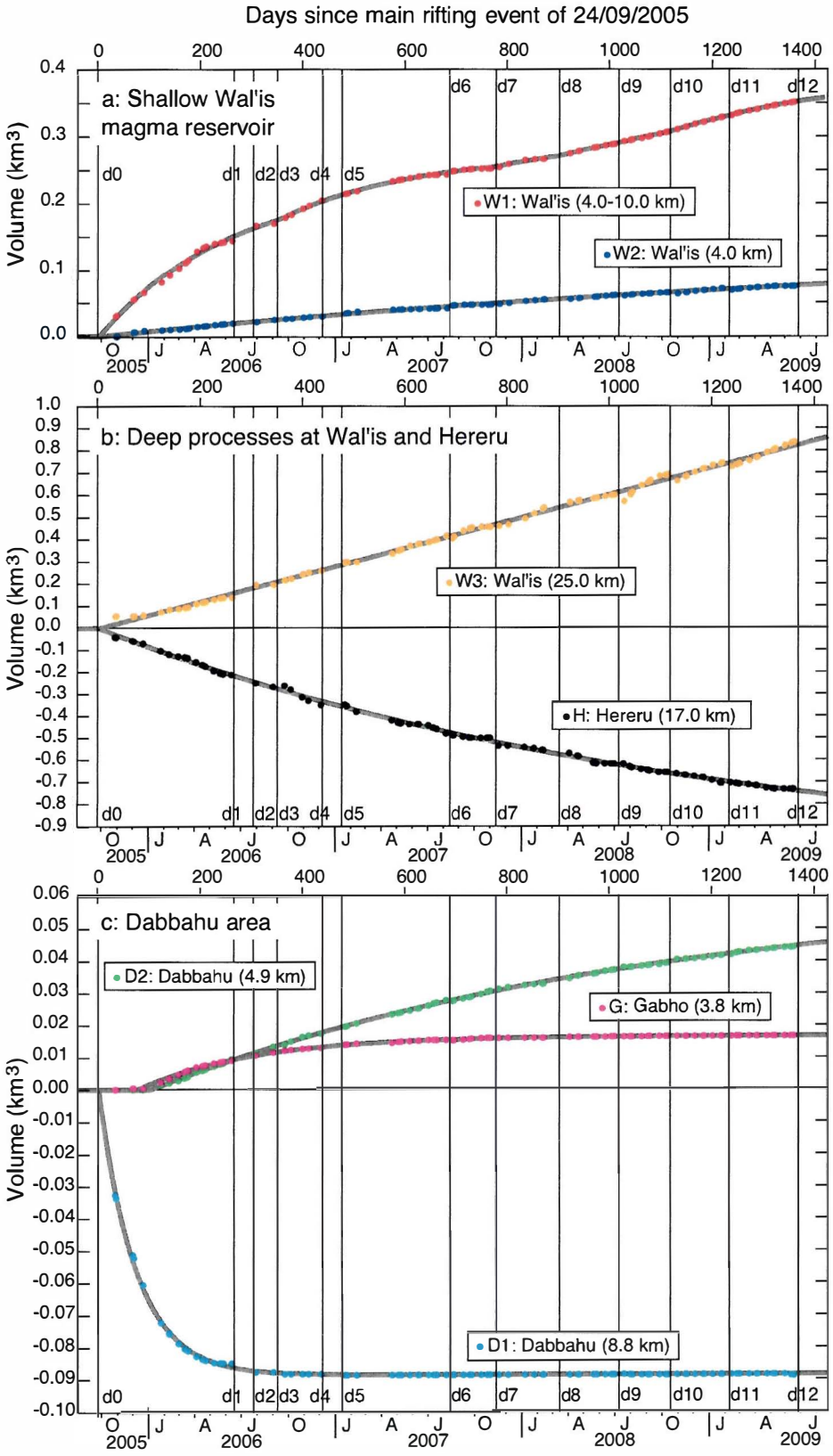

Figure 7. Source time functions deduced after fitting original STFs of Figure 5 (dots) with simple analytic functions (grey lines). The total cumulative volume of each source is deduced from elastic inversion and extrapolation with these simple functions.

Manda Hararo rift, with the exception of the first rifting event of September 2005. This indicates that there exists no direct hydraulic connection at depth between these magma reservoirs and the central plumbing system of Manda Hararo after 2005.

5.3. Deformation at the Center of the Manda Hararo Rift

[31] Using surface displacement derived from GPS data acquired from late December 2005 in the vicinity of the Manda Hararo–Dabbahu rift, *Nooner et al.* [2009] measured a rift-perpendicular divergence that they interpreted as post-rifting visco-elastic relaxation at depth greater than 13 km. They were also able to explain surface displacement equally well by inflation of a deep dike at 20–25 km, embedded in an elastic half-space, a solution that they rejected because it requires sustained inflation within the ductile upper mantle, which is thought to be mechanically implausible. The new InSAR data set that we present in this study, which contains both ascending and descending InSAR data, allows us to better constrain deformation in the near-field. Using this data set, we propose an alternative interpretation of the processes of inflation at shallow depth in the Manda Hararo rift, in the period following the September 2005 mega-dike intrusion. We suggest that deformation affecting the central part of the Manda Hararo–Dabbahu rift is caused by transient inflation of a mid-segment magma reservoir which, at shallow depth (4–10 km), may be modeled as a composite dike/Mogi source (sources W1 and W2). At greater depth (W3: 25 km), deep inflation is detected, but additional data is required to understand better this latter source of deformation, and the contribution of each source to the deformation measured by GPS at distance greater than 25 km (Figure 3).

[32] The time series deduced from section 4 show that the rate of the horizontal component of inflation at source W1 increases sharply after the dike intrusions (Figure 6). Repeated dike intrusions from 2005 to 2009 seem to have triggered this transient behavior. Furthermore, the inferred source of this signal (W1) is spatially correlated with a focused mid-segment magma supply [*Keir et al.*, 2009] (Figure 1), and is located in the area where the plate boundary is not affected by any discrete diking event at depths greater than ~4 km (maximum dike intrusions further north or south occur down to ~12 km) [*Grandin et al.*, 2010]. Assuming that the observed transient deformation reflects the response of this central magma reservoir to internal pressure change (either directly, or indirectly due to hydraulic connectivity), the time evolution of this inflation signal is similar to that observed and modeled by *Lengliné et al.* [2008] after eruptions at Mauna Loa (Hawaii) and Piton de la Fournaise (La Réunion). A model of magma inflow driven by the pressure difference between the shallow inflating reservoir and a larger, probably deeper, magma reservoir with constant overpressure, predicts an exponential decay of the inflation rate [e.g., *Dvorak and Okamura*, 1987; *Lengliné et al.*, 2008].

[33] However, the dominant mode of deformation in the center of the Manda Hararo rift differs significantly from that produced by a nearly spherical magma reservoir, which is the shape of magma storage generally assumed for most volcanoes in the world. We propose a composite sill/dike source of deformation (sources W1 and W2) at 4–10 km depth, with the 8 km-long dike component dominating the budget of inflation. This geometry may be typical of magmatic rift segments near their mid-segment magma supply. Indeed, the area affected by transient rift opening occurs where focused melt supply to the magmatic segment is inferred from seismological, geodetic, geological and structural observations [*Rowland et al.*, 2007; *Ebinger et al.*, 2008; *Keir et al.*, 2009; *Grandin et al.*, 2009]. Similar central magma reservoirs have been detected on second-order segments of the slow-spreading Mid-Atlantic Ridge. With respect to segment ends, the mid-segment magma reservoirs are often associated with a negative mantle Bouguer gravity anomaly, a low-velocity anomaly, and a shallowing of the axial valley [e.g., *Lin et al.*, 1990; *Tolstoy et al.*, 1993]. These anomalies are interpreted as a greater thickness of the crust at segment center, due to higher melt supply, in comparison to segment ends, where large throw normal faults, sometimes associated with exhumation of mantle rocks, has been reported [e.g., *Cannat*, 1996]. For the well-studied OH1 segment of the Mid-Atlantic Ridge, which shares many structural analogies with the Manda Hararo–Dabbahu rift, seismic tomography images this mid-segment magma supply as a vertical pipe-like low-velocity anomaly in the lower crust (>4.0 km depth) [*Magde et al.*, 2000; *Dunn et al.*, 2005]. A similar pipe-like low-velocity anomaly at the center of the Asal Quaternary magmatic segment (Afar) has been detected [*Doubre et al.*, 2007a, 2007b], possibly connected to the magma reservoir that fed the dikes of the 1978 "Ardoukôba" rifting event [*Abdallah et al.*, 1979; *Tarantola et al.*, 1980]. There, rift opening has occurred largely aseismically from 1979 to 1986 at twice the plate divergence rate [e.g., *Ruegg and Kasser*, 1987]. This accelerated opening is better explained by deep dike inflation than post-rifting relaxation [*Cattin et al.*, 2005]. We propose that the transient inter-diking deformation that we have monitored in the center of the Manda Hararo–Dabbahu rift is also explained by dike-like inflation of the main mid-segment magma reservoir as a result of tectonic divergence across the plate boundary.

[34] In addition, the composite dike/Mogi source that we have determined by inversion of InSAR data has already been proposed by others in similar environments. In the Krafla rift segment (Iceland) during the period 1993–1999, *de Zeeuw-van Dalfsen et al.* [2004] have observed a broad uplift that they interpret as being produced by magma accumulation at the crust-mantle boundary at 21 km depth, associated with an asymmetry of the fringe pattern induced by an horizontal opening across the rift, possibly caused by localized plate divergence. More recently, *Amelung et al.* [2007] have interpreted the rift opening observed at Mauna Loa (Hawaii) from 2002 to 2005 as being caused by the inflation of a dike-like magma body at 5 km depth, superimposed in space with a spherical inflating magma reservoir. The fringe pattern and the transient nature of the deformation described in these two studies strikingly resembles that found at Manda Hararo; unfortunately, the time evolution of these sources is not available. Nevertheless, transient deformation in 1997 at Kilauea (Hawaii) has been deduced from continuous GPS data by *Desmarais and Segall* [2007]

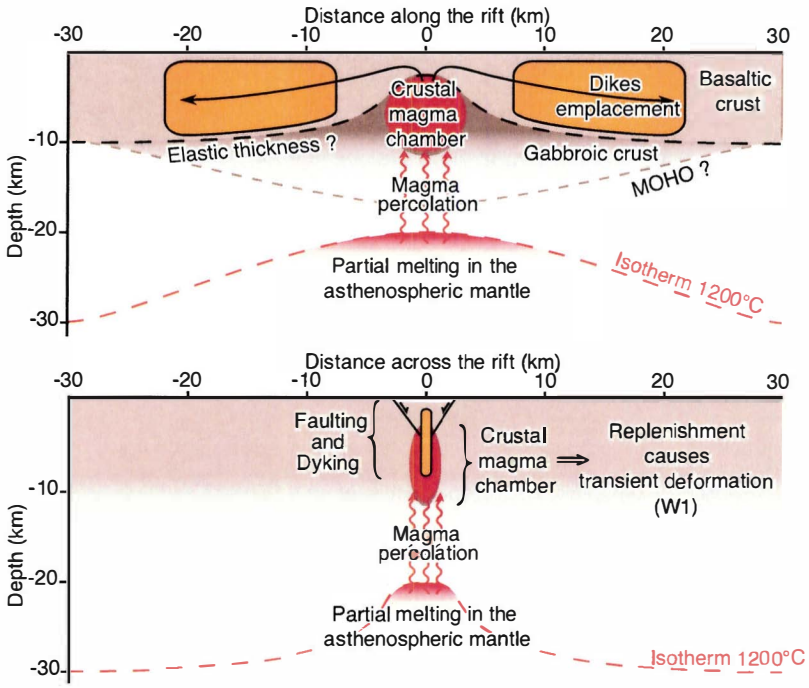

Figure 8. Proposed lithological and mechanical structure of the Manda Hararo rift: (top) along-axis profile and (bottom) transverse profile. Partial melting in a locally shallower asthenosphere, results in magma percolation in the lower crust and magma accumulation in a crustal reservoir at the center of the rift. Magma is episodically distributed along the segment by repeated lateral dike injections, inducing a sudden deflation of the central magma reservoir. Rapid replenishment of the reservoir leads to transient phases of inflation of an axial dike-like body, with ambient rift-perpendicular tensional tectonic stress forcing a predominantly horizontal mode of deformation during inflation.

in an environment analogue to that of Mauna Loa and Piton de la Fournaise. This transient signal exhibits a great similarity with that of Manda Hararo, with a decaying rate of inflation of a dike-like source during the few months following a dike intrusion. This behavior may be typical of the post-intrusive response of the central plumbing system in the context of magma-assisted rifting.

[35] These results may be interpreted in the following way (Figure 8). In presence of a tensional tectonic stress (as can be inferred at Manda Hararo until 2009 by the occurrence of repeated dike injections, but also by the divergence of Nubia/Arabia plates), continuous opening at depth may occur in response to magma ascent into the magma reservoir lying at the base of the elastic-brittle crust. The preferential rift-perpendicular direction of deformation is probably controlled by the direction of the least compressive principal stress induced by tectonic (in Afar and Iceland) or gravitational (at Hawaii and La Réunion) effects. This direction, approximately perpendicular to the direction of the rift, would explain the shape of the shallow magma reservoir that would open as a fluid-filled tension crack. This response may be further boosted by lubrication and/or hydraulic fracturing induced by rapid magma inflow in the source region as a result of co-diking pressure drop and/or poroelastic effects. Also, in analogy to mid-ocean ridges, the strongly anisotropic structure of the lithosphere both across and along the rift axis [e.g., *Cannat*, 1996; *Dunn et al.*, 2005] may enhance the localization of this deformation transient. So, as the dynamics of deformation may be controlled by fluid migration processes (magmatic connection between different reservoirs), the mode of deformation is forced to obey the strongly tensional stress state that prevails in the surrounding solid earth as a result of divergent tectonic forcing. The progressively decreasing ratio between the horizontal component of deformation at W1 and the vertical component at W2 (Figure 5) may reflect the gradual decrease of the intensity of the rift-perpendicular stress as this stress is accommodated by the intrusion of the successive instantaneous or transient dike bodies. During a dike intrusion, deflation of the dike-like magma reservoir is not observed, suggesting that this deformation is not recoverable when magma is drained. A similar hysteretic behavior was observed at Krafla (Iceland) and Kilauea (Hawaii) throughout repeated cycles of slow inflation of the rift zone and rapid deflation due to either dike intrusions or volcanic eruptions [*Ewart et al.*, 1991; *Yang et al.*, 1992]. In our view, this supports the hypothesis that accretion of mafic material operates not only in the upper crust by discrete dike intrusions, but also at deeper levels, where tensional stresses induce slow dike-like inflation of the plate boundary. Although usually rejected based on thermal or mechanical considerations, and generally considered to play a negligible role in comparison to distributed, isochoric, plastic deformation (viscous relaxation) [e.g., *Nooner et al.*, 2009], we suggest that dike-like inflation at depth greater than the thickness of the brittle-elastic crust, may be an efficient mechanism of

accretion of the oceanic crust if sufficient magma is available to accommodate the tectonic strain. Enhanced melt supply, such as that occurring near the center of a magmatic rift, may provide conditions for this process to become predominant over distributed viscous relaxation.

5.4. Relationship Between Deep Sources of Deformation at Wal'is and Hereru

[36] Following the emplacement of the September 2005 mega-dike, onset of a broad subsidence signal is observed in the Hereru area (H). Similarly, a broad inflation is detected in the Wal'is area (W3). Both sources lie at depths greater than 15 km (17 km for H, 25 km for W3, according to our inversions), but the depth is poorly constrained. However, the physical process responsible for these deformation signals is unknown, although they are likely to be related to the response of the lithosphere to influx or withdrawal of subcrustal material.

[37] Similar observations were made in the neighboring magmatic segments of Krafla and Askja, in the Northern Volcanic Zone of Iceland. Using GPS, InSAR and gravity measurements at Askja volcano, it was proposed that, approximately coeval to the onset of the 1975–1984 rifting episode that affected the magmatic segment of Krafla, a deep deflation (16 km depth) initiated below the Askja central volcano. This transient signal has continued at a decaying rate in the following decades [*Pagli et al.*, 2006; *de Zeeuw-van Dalfsen et al.*, 2006; *Sturkell et al.*, 2006]. The deflation may have been caused by drainage of a deep magma reservoir into the expanding plate boundary in the ductile lower crust or at crust-mantle boundary. Deformation in the Hereru area may be another example of the phenomenon observed at Askja. This is supported by the location of Hereru, at the center of the Southern Manda Hararo magmatic segment [e.g., *Tazieff et al.*, 1972; *Barberi et al.*, 1972; *Manighetti et al.*, 2001; *Grandin et al.*, 2009]. The similarity between the onset of a rifting episode on a magmatic segment (Manda Hararo or Krafla), and the triggered response of a nearby central volcano (Hereru or Askja) is striking.

[38] As a concluding remark, we notice that the deep inflation at Wal'is (W3) and the deep deflation at Hereru (H) both appear to evolve on long time-scales (perhaps of the order of tens of year), and with nearly equal rates of volume change (± 0.2 km^3/yr). The volume balance between the two inferred magma reservoirs is crudely satisfied, possibly suggesting that the two sources are hydraulically connected, although the mechanism of interaction between them is not understood.

6. Conclusions

[39] In this paper, taking advantage of an extensive InSAR data set, we have produced time series of deformation occurring in the Manda Hararo–Dabbahu rift, Afar (Ethiopia), in the inter-diking intervals separating thirteen dike intrusions. To link the four data sets originating each from a different InSAR track, elastic analytic functions were used. This allowed us to increase the temporal sampling compared to a classical pixel-by-pixel time series, and to separate the contribution of seven sources of deformation that may have been difficult to distinguish if only one look-angle had been used.

[40] At the extremity of the magmatic segment, in the Dabbahu–Gabho area, three slowly evolving magma reservoirs are detected. At Dabbahu, 6 months of deep deflation seem to reflect the maintained connectivity of a magma reservoir with the mega-dike emplaced in September 2005. From January 2006, inflation initiates at Dabbahu at a shallower level, first at a fast rate, and then decelerating until 2009. The satellite magma reservoir of Gabho, which also deflated during the main 2005 rifting event, has re-inflated since late 2005, until late 2007. The evolution of inflation of these magma reservoirs seems to be unaffected by dike intrusions occurring ~30–60 km further south in 2006–2008, and can be interpreted as a standard post-eruptive pressure re-equilibration between shallow and deep magma reservoirs.

[41] In contrast, a complex spatial and temporal pattern of deformation is detected in the center of the Manda Hararo rift, at the location of the inferred magma supply for the 2005–2009 dikes. A moderate uplift of deep origin (~25 km) is observed from September 2005, until at least 2009, with a nearly constant rate. This signal may be related to magma accumulation at the crust-mantle boundary following the massive extrusion of material from the central magma reservoir, and the emplacement of magma into the mega-dike ~10–20 km further north. In contrast, a horizontal component of deformation of shallow origin (4–10 km) exhibits a series of pulses after most of the dike intrusions of 2006–2009. A gradual decay of the rate of localized horizontal opening is then observed in the months following each diking event. Colocated with this dike-like body, a Mogi-like magma reservoir at 4 km depth may be inflating at a nearly constant rate between dike intrusions, and may provide the material emplaced in the dikes. The transient horizontal deformation events on the plate boundary are interpreted as the result of post-intrusion mode I inflation triggered by a rapid influx of magma into the region underlain by the mid-segment magma reservoir, in presence of a tensional stress field.

[42] A nearly steady state subsidence signal of deep origin is also detected on a neighboring rift segment (Hereru) throughout the period, and could be interpreted as a broad source of deflation. This deflation may be related to the lateral transfer of magma between the two rift segments, possibly along the crust-mantle boundary.

Appendix A: Notation

[43] In the following, matrixes are represented by boldface letters, whereas elements of a matrix are indicated by plain letters, with the subscripts or superscripts giving the coordinates of the element within the matrix. Matrix elements with two subscripts refer to a full matrix, and elements with one subscript and one superscript belong to a column vector. Spatial vectors are identified by overlying arrows. The dot is the term-by-term scalar multiplication, unless when applied to matrixes, where it stands for matrix multiplication. The symbols $\langle , \rangle$ are used for the scalar product between two vectors. The Einstein summation convention is not used.

[44] The signification of indexes is as follows: the letter i is used to refer to an interferogram, the letter k is used to refer to a point of the Earth's surface, the letter j is used to refer to a source of deformation, and the letter l is used to refer to a date of SAR acquisition.

Appendix B: Time Series Inversion

B1. Direct problem

[45] For interferogram I_i, which spans the deformation of the ground surface between the dates T_i^a and T_i^b (with $T_i^a < T_i^b$), the (scalar) LOS displacement d_i^k at point P^k is given by

$$d_i^k = \langle \vec{u}_i^k, \vec{V}_i^k \rangle + \epsilon_i^k \tag{B1}$$

where $\vec{u}_i^k$ is the unit vector at P^k pointing toward the satellite, $\vec{V}_i^k$ is the cumulative surface displacement at P^k between the dates T_i^a and T_i^b, and ϵ_i^k is the perturbation of the signal induced by all other phenomena (such as atmospheric effects, unmodeled deformation, unwrapping errors, orbit uncertainties, errors in the DEM), assumed to be small compared to d_i^k.

[46] We assume that surface displacement $\vec{V}_i^k$ is caused by the contribution of J sources:

$$\vec{V}_i^k = \sum_{j=1}^{J} \{a_i^j . \vec{g}^{jk}\} \tag{B2}$$

where a_i^j is the cumulative activity of source j (the so-called "source time function", STF) between the dates T_i^a and T_i^b, and $\vec{g}^{jk} = \vec{f}(P^k, \tau^j)$ is the Green's function giving the displacement produced at P^k by a unit increment of activity of source j. The vector τ_j contains all the information relevant to the description of source j (e.g., geometry, mode of deformation).

[47] The activity of source j during the interval of time spanned by interferogram I_i can be written

$$a_i^j = \sum_{l'=t_i^a}^{t_i^b - 1} \{m_l^j . (\Theta_{l+1} - \Theta_l)\} \tag{B3}$$

where Θ is a column vector containing the L dates of SAR acquisitions, in chronological order, t_i^a and t_i^b are the indexes in Θ corresponding to the dates of acquisition of the two images used to produce interferogram I_i (dates T_i^a and T_i^b are given by $T_i^a = \Theta_{t_i^a}$ and $T_i^b = \Theta_{t_i^b}$), and m_l^j is the rate of activity of source j between two successive dates Θ_l and Θ_{l+1}.

[48] Information about dates of acquisitions of InSAR images can be conveniently grouped into a matrix $\mathbf{K}$, defined by

$$K_{il} = \begin{cases} 1 & \text{if} \quad T_i^a \le \Theta_l < T_i^b \\ 0 & \text{elsewhere} \end{cases} \tag{B4}$$

so that the expression of a_i^j in equation (B3) can be rewritten

$$a_i^j = \sum_{l=1}^{L-1} \{K_{il} . m_l^j . (\Theta_{l+1} - \Theta_l)\} \tag{B5}$$

The direct problem can thus be written in matrix form:

$$\mathbf{d} = \mathbf{G} \cdot \mathbf{m} \tag{B6}$$

where $\mathbf{d}$ is the vector containing the data points d_i^k and $\mathbf{m}$ is the vector containing the model parameters m_l^j, which correspond, here, to the rate of activity of each source, in each time interval. Matrix $\mathbf{G}$ is the data kernel, which combines knowledge about the geometries of acquisition ($\mathbf{u}$), the list of dates at which the STF must be calculated ($\mathbf{\Theta}$), the Green's functions ($\mathbf{g}$), and the time spanned by each interferogram ($\mathbf{K}$):

$$G_{il}^{jk} = \langle \vec{u}_i^k \cdot \vec{g}^{jk} \rangle \cdot \sum_{l=1}^{L-1} \{K_{il} \cdot (\Theta_{l+1} - \Theta_l)\} \tag{B7}$$

[49] We aim to use a simplified model to link the tracks together in order to monitor the evolution of deformation with a fine sampling in time. In order to combine interferograms originating from different tracks in the inversion of the STFs, one must choose an explicit formulation for $\mathbf{g}$ (equation (B2)). Any kind of model can be used to describe the direct problem, as long as deformation of the surface is proportional to the activity of the source.

[50] Because of their simplicity, we choose to use elastic Green's functions, although we do not believe that the processes studied in this paper can be fully described by the elastic theory. The Earth is modeled as a homogeneous, isotropic, linear elastic half-space, with a Poisson's ratio of 0.25. Topography of the surface of the Earth is not taken into account.

[51] The analytic formulas of *Okada* [1985] give the deformation of the surface induced by the unit incremental activity (here, either inflation or deflation) of a rectangular dislocation of arbitrary geometry. In complement, the solution of *Mogi* [1958] is used to describe the displacement field caused by a unit volume change within a spherical point-source. Each source is described by a set of geometric parameters: position in the three coordinates of space (x^j, y^j, z^j), strike (φ^j), dip (δ^j), width (W^j), length (L^j). For the Mogi source, only the position of the point source is defined (x^j, y^j, z^j), and deformation is proportional to the volume change of the source, which is the parameter incorporated in $\mathbf{m}$. The Green's function thus becomes

$$\vec{g}^{jk} = \vec{f}(P^k, \tau^j) = \vec{f}_{Elastic}(x^k, y^k, x^j, y^j, z^j, \varphi^j, \delta^j, W^j, L^j) \tag{B8}$$

where the parameters in τ^j are chosen by a preliminary inversion.

[52] Because there is no common SAR scene for interferograms acquired on different tracks, an unconstrained inversion of equation (B6) using the raw definition of the data kernel $\mathbf{G}$ defined in equation (B7) leads to strong steps in the STFs between two successive acquisitions belonging to different tracks, even if they are separated by only a few days. In order to tackle this effect, a smoothing scheme in time is required. We introduce a smoothness matrix $\mathbf{G}_{smooth}$ containing first-order time derivatives approximated by a two-point 1D backward difference operator, applied on each interval between two successive acquisition dates. Because the inverted parameters m_l^j are already time derivatives of the amount of activity of each source, this scheme is in fact equivalent to a second-order smoothing in time (i.e. variations of inflation or deflation rate are required to be slow). We also invert for an offset and planar trend (three para-

meters per interferogram) in order to model and correct possible residual orbital errors.

[53] The direct problem finally becomes

$$\begin{bmatrix} \mathbf{d} \\ 0 \end{bmatrix} = \begin{bmatrix} \mathbf{G} & \mathbf{G}_{orbit} \\ \gamma \cdot \mathbf{G}_{smooth} & 0 \end{bmatrix} \cdot \begin{bmatrix} \mathbf{m} \\ \mathbf{m}_{orbit} \end{bmatrix} \quad \text{(B9)}$$

where γ is a scalar controlling the amount of smoothness of the solution (unit: m/s^{-2} or m^3/s^{-2}, depending on the parameter that describes the activity of the sources), and $\mathbf{m}$ is the column vector of STF for all sources (one parameter per source, for each time interval). $\mathbf{G}_{orbit}$ is the matrix containing the LOS phase perturbation induced by orbital errors in $\mathbf{m}_{orbit}$ calculated at P^k. Here, we invert for a residual offset and plane, but additional effects can be modeled, such as topography-correlated tropospheric delay, or DEM errors. These can be included in the inversion by modifying $\mathbf{G}_{orbit}$.

B2. Inversion Procedure

[54] Prior to inversion, each interferogram is downsampled, with the double objective of reducing the number of points in the inversion, and giving more weight to the areas affected by deformation. For most images, this produces an increase of the standard deviation of the distribution of data points from nearly 1.3 cm to 3.0 cm on average, while the number of points is reduced from over 10^6 to nearly 500.

[55] A preliminary non-linear inversion [*Tarantola and Valette*, 1982] is performed to determine the optimal values of the parameters in $\vec{g}^{jk}$ (section 3.1). Once these parameters are fixed, the problem become linear. The linear inverse problem is overdetermined and is solved in the least squares sense [*Menke*, 1989]. A non-negativity constraint is imposed on $\mathbf{m}$ in order to further reduce the oscillatory behavior of the solutions. This constraint is relaxed for inversions with a strong smoothing, which can be performed using a regular least squares inversion, in order to enhance computational efficiency. This inversion scheme is applied independently on each interval of time separating two successive dike intrusions.

[56] Various values of γ are tested (Figure S8). A large γ corresponds to a steady state STF, whereas a low γ produces large steps between successive closely spaced acquisition dates. This is caused by the irregular sampling of the time series in the available SAR archive. The preferred value of γ is chosen so that changes of rate of activity of any source over a period of less than 1 month are not taken into account, thus focusing on longer-term variations of activity.

[57] After the inversion, the standard deviation of the input data vector $\mathbf{d}$ is 3.34 cm, and the residual vector has a standard deviation of 1.04 cm. For most individual interferograms, the standard deviation of the residues (i.e. downsampled LOS data minus predicted LOS deformation) drops to less than 1.0 cm, presumably reflecting the level of uncertainty in the modeling (Figure S9 and Table S2). Only two interferograms show a larger residual (>2.5 cm), but they span partly the period that follows closely the September 2005 mega-dike, when additional unmodeled processes of deformation, such as viscous relaxation in the mantle and continued mega-dike inflation in the northern part of the Manda Hararo rift, may have been important [*Nooner et al.*, 2009].

Appendix C: Exponential Decay of Post-rifting Response

[58] We focus on the response of a given source j to a series of dike intrusions (subscript j is dropped for clarity). For this source, following the nth dike intrusion that occurred at the date T_n^0, the rate of activity μ_n (homogeneous to m_l) as a function of time t is assumed to obey an exponential decay function of amplitude O_n and time constant τ:

$$\mu_n(t) = \mathcal{H}\left(t - T_n^0\right) \cdot O_n \cdot e^{-\frac{t-T_n^0}{\tau}} \quad \text{(C1)}$$

where $\mathcal{H}$ is the Heaviside step function. The response to a sequence of N dikes can thus be written in matrix form as

$$\mathbf{B} = [\mathbf{E} \quad \mathbf{H}] \cdot \begin{bmatrix} \mathbf{O} \\ \mathbf{S} \end{bmatrix} \quad \text{(C2)}$$

where $\mathbf{H}$ is the Heaviside operator:

$$H_{nl} = \begin{cases} 1 & if \quad \Theta_l \geq T_n^0 \\ 0 & \text{elsewhere} \end{cases} \quad \text{(C3)}$$

and $\mathbf{E}$ is an operator that combines the exponential response function and the Heaviside function:

$$E_{nl} = \begin{cases} e^{-\frac{\Theta_l - T_n^0}{\tau}} & if \quad \Theta_l \geq T_n^0 \\ 0 & \text{elsewhere} \end{cases} \quad \text{(C4)}$$

[59] Vector $\mathbf{B}$ in equation (C2) is the data vector containing the L-1 terms of the cumulative activity of the source of interest deduced from the elastic inversion (Appendix B):

$$B_l = \sum_{l'=1}^{t_l - 1} \{m_{l'} \cdot (\Theta_{l'+1} - \Theta_{l'})\} \quad \text{(C5)}$$

Vector $\mathbf{O}$ is the vector of unknown O_n. Vector $\mathbf{S}$ is the vector containing unknown offsets B_l that account for the unknown activity occurring between T_n^0 and the first element in Θ satisfying $\Theta_l \geq T_n^0$.

[60] With this formulation, the direct problem is linear, and the inverse problem is solved in the least squares sense [*Menke*, 1989] for various values of τ, and the best τ is chosen as the one that minimizes the RMS misfit between activity of sources deduced from the time series inversion, and the activity predicted by the analytic functions described above (Figure S10).

[61] **Acknowledgments.** We thank Cécile Doubre, Cécile Lasserre, Alexandre Nercessian, Paul Tapponnier, Benoît Taisne and Steve Tait for fruitful discussions and suggestions. We thank Arthur Delorme and Geneviève Moguilny, who provided assistance for the InSAR processing. We thank two anonymous reviewers for their constructive remarks that helped to improve the manuscript. We thank the European Space Agency (ESA) for programming the Envisat satellite and providing data crucial to this work (AOE-272, AOE-720 and PNTS project "Télédétection des déformations transitoires"). The Repeat Orbit Interferometry Package (ROI_PAC) software was provided by Caltech/Jet Propulsion Laboratory (JPL). Most figures were prepared with the Generic Mapping Tool (GMT) software by *Wessel and Smith* [1991]. This is IPGP contribution 3000.

References

Abdallah, A., V. Courtillot, M. Kasser, A.-Y. Le Dain, J.-C. Lépine, B. Robineau, J.-C. Ruegg, P. Tapponnier, and A. Tarantola (1979), Relevance of Afar seismicity and volcanism to the mechanics of accreting plate boundaries, *Nature*, *282*, 17–23, doi:10.1038/282017a0.

Amelung, F., S.-H. Yun, T. R. Walter, P. Segall, and S.-W. Kim (2007), Stress control of deep rift intrusion at Mauna Loa Volcano, Hawaii, *Science*, *316*, 1026, doi:10.1126/science.1140035.

Armijo, R., B. Meyer, G. C. P. King, A. Rigo, and D. Papanastassiou (1996), Quaternary evolution of the Corinth Rift and its implications for the Late Cenozoic evolution of the Aegean, *Geophys. J. Int.*, *126*, 11–53, doi:10.1111/j.1365-246X.1996.tb05264.x.

Ayele, A., E. Jacques, M. Kassim, T. Kidane, A. Omar, S. Tait, A. Nercessian, J.-B. de Chabalier, and G. C. P. King (2007), The volcano seismic crisis in Afar, Ethiopia, starting September 2005, *Earth Planet. Sci. Lett.*, *255*, 177–187, doi:10.1016/j.epsl.2006.12.014.

Ayele, A., D. Keir, C. Ebinger, T. J. Wright, G. W. Stuart, W. R. Buck, E. Jacques, G. Ogubazghi, and J. Sholan (2009), September 2005 mega-dike emplacement in the Manda-Harraro nascent oceanic rift (Afar depression), *Geophys. Res. Lett.*, *36*, L20306, doi:10.1029/2009GL039605.

Barberi, F., H. Tazieff, and J. Varet (1972), Volcanism in the Afar depression: Its tectonic and magmatic significance, *Tectonophysics*, *15*, 59–64, doi:10.1016/0040-1951(72)90051-0.

Beauducel, F., P. Briole, and J.-L. Froger (2000), Volcano-wide fringes in ERS synthetic aperture radar interferograms of Etna (1992–1998): Deformation or tropospheric effect?, *J. Geophys. Res.*, *105*, 16,391–16,402, doi:10.1029/2000JB900095.

Berardino, P., G. Fornaro, R. Lanari, and E. Sansosti (2002), A new algorithm for surface deformation monitoring based on small baseline differential SAR interferograms, *IEEE Trans. Geosci. Remote Sens.*, *40*, 2375–2383, doi:10.1109/TGRS.2002.803792.

Björnsson, A. (1985), Dynamics of crustal rifting in NE Iceland, *J. Geophys. Res.*, *90*(B12), 10,151–10,162, doi:10.1029/JB090iB12p10151.

Buck, W. R., P. Einarsson, and B. Brandsdóttir (2006), Tectonic stress and magma chamber size as controls on dike propagation: Constraints from the 1975–1984 Krafla rifting episode, *J. Geophys. Res.*, *111*, B12404, doi:10.1029/2005JB003879.

Cannat, M. (1996), How thick is the magmatic crust at slow spreading oceanic ridges?, *J. Geophys. Res.*, *101*, 2847–2857, doi:10.1029/95JB03116.

Cattin, R., C. Doubre, J. de Chabalier, G. King, C. Vigny, J. Avouac, and J. Ruegg (2005), Numerical modelling of quaternary deformation and post-rifting displacement in the Asal-Ghoubbet rift (Djibouti, Africa), *Earth Planet. Sci. Lett.*, *239*, 352–367, doi:10.1016/j.epsl.2005.07.028.

Cavalié, O., M.-P. Doin, C. Lasserre, and P. Briole (2007), Ground motion measurement in the Lake Mead area, Nevada, by differential synthetic aperture radar interferometry time series analysis: Probing the lithosphere rheological structure, *J. Geophys. Res.*, *112*, B03403, doi:10.1029/2006JB004344.

de Zeeuw-van Dalfsen, E., R. Pedersen, F. Sigmundsson, and C. Pagli (2004), Satellite radar interferometry 1993–1999 suggests deep accumulation of magma near the crust-mantle boundary at the Krafla volcanic system, Iceland, *Geophys. Res. Lett.*, *31*, L13611, doi:10.1029/2004GL020059.

de Zeeuw-van Dalfsen, E., H. Rymer, G. Williams-Jones, E. Sturkell, and F. Sigmundsson (2006), Integration of micro-gravity and geodetic data to constrain shallow system mass changes at Krafla Volcano, N Iceland, *Bull. Volcanol.*, *68*, 420–431, doi:10.1007/s0445-005-0018-5.

Delaney, P. T., R. S. Fiske, A. Miklius, A. T. Okamura, and M. K. Sako (1990), Deep magma body beneath the summit and rift zones of Kilauea Volcano, Hawaii, *Science*, *247*, 1311–1316, doi:10.1126/science.247.4948.1311.

Desmarais, E. K., and P. Segall (2007), Transient deformation following the 30 January 1997 dike intrusion at Kilauea volcano, Hawai'i, *Bull. Volcanol.*, *69*, 353–363, doi:10.1007/s00445-006-0080-7.

Dieterich, J. H., and R. W. Decker (1975), Finite element modeling of surface deformation associated with volcanism, *J. Geophys. Res.*, *80*, 4094–4102, doi:10.1029/JB080i029p04094.

Doin, M.-P., C. Lasserre, G. Peltzer, O. Cavalié, and C. Doubre (2009), Corrections of stratified tropospheric delays in SAR interferometry: Validation with global atmospheric models, *J. Appl. Geophys.*, *69*, 35–50, doi:10.1016/j.jappgeo.2009.03.010.

Doubre, C., and G. Peltzer (2007), Fluid-controlled faulting process in the Asal Rift, Djibouti, from 8 yr of radar interferometry observations, *Geology*, *35*, 69–72, doi:10.1130/G23022A.1.

Doubre, C., I. Manighetti, C. Dorbath, L. Dorbath, E. Jacques, and J.-C. Delmond (2007a), Crustal structure and magmato-tectonic processes in an active rift (Asal-Ghoubbet, Afar, East Africa): 1. Insights from a 5-month seismological experiment, *J. Geophys. Res.*, *112*, B05405, doi:10.1029/2005JB003940.

Doubre, C., I. Manighetti, L. Dorbath, C. Dorbath, D. Bertil, and J. C. Delmond (2007b), Crustal structure and magmato-tectonic processes in an active rift (Asal-Ghoubbet, Afar, East Africa): 2. Insights from the 23-year recording of seismicity since the last rifting event, *J. Geophys. Res.*, *112*, B05406, doi:10.1029/2006JB004333.

Dunn, R. A., V. Lekić, R. S. Detrick, and D. R. Toomey (2005), Three-dimensional seismic structure of the Mid-Atlantic Ridge (35°N): Evidence for focused melt supply and lower crustal dike injection, *J. Geophys. Res.*, *110*, B09101, doi:10.1029/2004JB003473.

Dvorak, J. J., and A. T. Okamura (1987), A hydraulic model to explain variations in summit tilt rate at Kilauea and Mauna-Loa volcanoes, in *Volcanism in Hawaii*, *U.S. Geol. Surv. Prof. Pap.*, 1350, 1281–1296.

Dzurisin, M. (2006), *Volcano Deformation: Geodetic Monitoring Techniques*, Springer, Berlin.

Ebinger, C. J., D. Keir, A. Ayele, E. Calais, T. J. Wright, M. Belachew, J. O. S. Hammond, E. Campbell, and W. R. Buck (2008), Capturing magma intrusion and faulting processes during continental rupture: seismicity of the Dabbahu (Afar) rift, *Geophys. J. Int.*, *174*, 1138–1152, doi:10.1111/j.1365-246X.2008.03877.x.

Einarsson, P., and B. Brandsdöttir (1980), Seismological evidence for lateral magma intrusion during the July 1978 deflation of the Krafla volcano in NE-Iceland, *J. Geophys.*, *47*, 160–165.

Ewart, J. A., B. Voight, and A. Björnsson (1991), Elastic deformation models of Krafla Volcano, Iceland, for the decade 1975 through 1985, *Bull. Volcanol.*, *53*, 436–459, doi:10.1007/BF00258184.

Farr, T. G., and M. Kobrick (2001), The Shuttle Radar Topography Mission, *Eos Trans. AGU*, *82*(47), Fall Meet. Suppl., Abstract G22B-0214.

Fialko, Y., Y. Khazan, and M. Simons (2001a), Deformation due to a pressurized horizontal circular crack in an elastic half-space, with applications to volcano geodesy, *Geophys. J. Int.*, *146*(1), 181–190, doi:10.1046/j.1365-246X.2001.00452.x.

Fialko, Y., M. Simons, and D. Agnew (2001b), The complete (3-D) surface displacement field in the epicentral area of the 1999 M_w 7.1 Hector Mine earthquake, California, from space geodetic observations, *Geophys. Res. Lett.*, *28*(16), 3063–3066, doi:10.1029/2001GL013174.

Goldstein, R. M., H. A. Zebker, and C. L. Werner (1988), Satellite radar interferometry—Two-dimensional phase unwrapping, *Radio Sci.*, *23*, 713–720, doi:10.1029/RS023i004p00713.

Grandin, R., et al. (2009), September 2005 Manda Hararo-Dabbahu rifting event, Afar (Ethiopia): Constraints provided by geodetic data, *J. Geophys. Res.*, *114*, B08404, doi:10.1029/2008JB005843.

Grandin, R., A. Socquet, E. Jacques, N. Mazzoni, J. B. de Chabalier, and G. C. P. King (2010), Sequence of rifting in Afar, Manda-Hararo rift, Ethiopia, 2005–2009: Time-space evolution and interactions between dikes from interferometric synthetic aperture radar and static stress change modeling, *J. Geophys. Res.*, doi:10.1029/2009JB000815, in press.

Hamling, I. J., A. Ayele, L. Bennati, E. Calais, C. J. Ebinger, D. Keir, E. Lewi, T. J. Wright, and G. Yirgu (2009), Geodetic observations of the ongoing Dabbahu rifting episode: New dyke intrusions in 2006 and 2007, *Geophys. J. Int.*, *178*, 989–1003, doi:10.1111/j.1365-246X.2009.04163.x.

Jónsson, S., H. Zebker, P. Segall, and F. Amelung (2002), Fault slip distribution of the 1999 M_w 7.1 Hector Mine, California, earthquake, estimated from satellite radar and GPS measurements, *Bull. Seismol. Soc. Am.*, *92*(4), 1377–1389, doi:10.1785/0120000922.

Keir, D., et al. (2009), Evidence for focused magmatic accretion at segment centers from lateral dike injections captured beneath the Red Sea rift in Afar, *Geology*, *37*(1), 59–62, doi:10.1130/G25147A.1.

Lengliné, O., D. Marsan, J.-L. Got, V. Pinel, V. Ferrazzini, and P. G. Okubo (2008), Seismicity and deformation induced by magma accumulation at three basaltic volcanoes, *J. Geophys. Res.*, *113*, B12305, doi:10.1029/2008JB005937.

Lin, J., G. M. Purdy, H. Schouten, J.-C. Sempere, and C. Zervas (1990), Evidence from gravity data for focused magmatic accretion along the Mid-Atlantic Ridge, *Nature*, *344*, 627–632, doi:10.1038/344627a0.

Lu, Z., T. Masterlark, D. Dzurisin, R. Rykhus, and C. Wicks Jr. (2003), Magma supply dynamics at Westdahl volcano, Alaska, modeled from satellite radar interferometry, *J. Geophys. Res.*, *108*(B7), 2354, doi:10.1029/2002JB002311.

Lundgren, P., S. Usai, E. Sansosti, R. Lanari, M. Tesauro, G. Fornaro, and P. Berardino (2001), Modeling surface deformation observed with synthetic aperture radar interferometry at Campi Flegrei caldera, *J. Geophys. Res.*, *106*, 19,355–19,366, doi:10.1029/2001JB000194.

Macdonald, K. C. (1982), Mid-ocean ridges: Fine scale tectonic, volcanic and hydrothermal processes within the plate boundary zone, *Annu. Rev. Earth Planet. Sci.*, *10*, 155, doi:10.1146/annurev.ea.10.050182.001103.

Magde, L. S., A. H. Barclay, D. R. Toomey, R. S. Detrick, and J. A. Collins (2000), Crustal magma plumbing within a segment of the Mid-Atlantic

Ridge, 35°N, *Earth Planet. Sci. Lett.*, *175*, 55–67, doi:10.1016/S0012-821X(99)00281-2.

Manighetti, I., P. Tapponnier, V. Courtillot, Y. Gallet, E. Jacques, and P.-Y. Gillot (2001), Strain transfer between disconnected, propagating rifts in Afar, *J. Geophys. Res.*, *106*, 13,613–13,666, doi:10.1029/2000JB900454.

Massonnet, D., and K. L. Feigl (1998), Radar interferometry and its application to changes in the Earth's surface, *Rev. Geophys.*, *36*, 441–500, doi:10.1029/97RG03139.

Menke, W. (1989), *Geophysical Data Analysis: Discrete Inverse Theory*, rev. ed., Academic, New York.

Mogi, K. (1958), Relations between the eruptions of various volcanoes and the deformations of the ground surfaces around them, *Bull. Earthquake Res. Inst. Univ. Tokyo*, *36*, 99–134.

Nooner, S. L., L. Bennati, E. Calais, W. R. Buck, I. J. Hamling, T. J. Wright, and E. Lewi (2009), Post-rifting relaxation in the Afar region, Ethiopia, *Geophys. Res. Lett.*, *36*, L21308, doi:10.1029/2009GL040502.

Okada, Y. (1985), Surface deformation to shear and tensile faults in a half space, *Bull. Seismol. Soc. Am.*, *75*(4), 1135–1154.

Pagli, C., F. Sigmundsson, T. Árnadóttir, P. Einarsson, and E. Sturkell (2006), Deflation of the Askja volcanic system: Constraints on the deformation source from combined inversion of satellite radar interferograms and GPS measurements, *J. Volcanol. Geotherm. Res.*, *152*, 97–108, doi:10.1016/j.jvolgeores.2005.09.014.

Pritchard, M. E., and M. Simons (2006), An aseismic slip pulse in northern Chile and along-strike variations in seismogenic behavior, *J. Geophys. Res.*, *111*, B08405, doi:10.1029/2006JB004258.

Rosen, P. A., S. Henley, I. R. Joughin, F. K. Li, S. N. Madsen, E. Rodríguez, and R. Goldstein (2000), Synthetic aperture radar interferometry, *Proc. IEEE*, *88*(3), 333–382.

Rosen, P. A., S. Henley, G. Peltzer, and M. Simons (2004), Updated repeat orbit interferometry package released, *Eos Trans. AGU*, *85*(5), 47, doi:10.1029/2004EO050004.

Rowland, J. V., E. Baker, C. J. Ebinger, D. Keir, T. Kidane, J. Biggs, N. Hayward, and T. J. Wright (2007), Fault growth at a nascent slow-spreading ridge: 2005 Dabbahu rifting episode, Afar, *Geophys. J. Int.*, *171*(3), 1226–1246, doi:10.1111/j.1365-246X.2007.03584.x.

Ruegg, J. C., and M. Kasser (1987), Deformation across the Asal-Ghoubbet rift, Djibouti, uplift and crustal extension 1979–1986, *Geophys. Res. Lett.*, *14*, 745–748, doi:10.1029/GL014i007p00745.

Schmidt, D. A., and R. Bürgmann (2003), Time-dependent land uplift and subsidence in the Santa Clara valley, California, from a large interferometric synthetic aperture radar data set, *J. Geophys. Res.*, *108*(B9), 2416, doi:10.1029/2002JB002267.

Simons, M., and P. A. Rosen (2007), Interferometric synthetic aperture radar, in *Treatise on Geophysics*, vol. 3, edited by G. Schubert, pp. 391–446, doi:10.1016/B978-044452748-6.00059-6, Elsevier, Amsterdam.

Simons, M., Y. Fialko, and L. Rivera (2002), Coseismic deformation from the 1999 M_w 7.1 Hector Mine, California, earthquake as inferred from InSAR and GPS observations, *Bull. Seismol. Soc. Am.*, *92*(4), 1390–1402, doi:10.1785/0120000933.

Smith, D. K., and J. R. Cann (1999), Constructing the upper crust of the Mid-Atlantic Ridge: A reinterpretation based on the Puna Ridge, Kilauea Volcano, *J. Geophys. Res.*, *104*, 25,379–25,399, doi:10.1029/1999JB900177.

Solomon, S. C., P. Y. Huang, and L. Meinke (1988), The seismic moment budget of slowly spreading ridges, *Nature*, *334*, 58–60, doi:10.1038/334058a0.

Sturkell, E., P. Einarsson, F. Sigmundsson, S. Hreinsdóttir, and H. Geirsson (2003), Deformation of Grímsvötnvolcano, Iceland: 1998 eruption and subsequent inflation, *Geophys. Res. Lett.*, *30*(4), 1182, doi:10.1029/2002GL016460.

Sturkell, E., F. Sigmundsson, and R. Slunga (2006), 1983 2003 decaying rate of deflation at Askja caldera: Pressure decrease in an extensive magma plumbing system at a spreading plate boundary, *Bull. Volcanol.*, *68*, 727–735, doi:10.1007/s00445-005-0046-1.

Tarantola, A., and B. Valette (1982), Generalized nonlinear inverse problems solved using the least squares criterion, *Rev. Geophys.*, *20*, 219–232, doi:10.1029/RG020i002p00219.

Tarantola, A., J.-C. Ruegg, and J.-C. Lépine (1980), Geodetic evidence for rifting in afar, 2. Vertical displacements, *Earth Planet. Sci. Lett.*, *48*, 363–370, doi:10.1016/0012-821X(80)90200-9.

Tazieff, H., J. Varet, F. Barberi, and G. Giglia (1972), Tectonic significance of the Afar (or Danakil) depression, *Nature*, *235*, 144–147, doi:10.1038/235144a0.

Tolstoy, M., A. J. Harding, and J. A. Orcutt (1993), Crustal thickness on the Mid-Atlantic Ridge: Bull's-eye gravity anomalies and focused accretion, *Science*, *262*, 726–729, doi:10.1126/science.262.5134.726.

Wessel, P., and W. H. F. Smith (1991), Free software helps map and display data, *Eos Trans. AGU*, *72*, 441, doi:10.1029/90EO00319.

Wright, T. J., C. Ebinger, J. Biggs, A. Ayele, G. J. Yirgu, D. Keir, and A. Stork (2006), Magma-maintained rift segmentation at continental rupture in the 2005 Afar dyking episode, *Nature*, *442*, 291–294, doi:10.1038/nature04978.

Yang, X., P. M. Davis, P. T. Delaney, and A. T. Okamura (1992), Geodetic analysis of Dike intrusion and motion of the magma reservoir beneath the summit of Kilauea Volcano, Hawaii: 1970–1985, *J. Geophys. Res.*, *97*, 3305–3324, doi:10.1029/91JB02842.

Zandbergen, R., P. Righetti, M. Otten, D. Kuijper, and J. Dow (2002), Routine operational and high-precision orbit determination of Envisat, paper presented at 34th COSPAR Scientific Assembly, Plenary Meeting, COSPAR, Houston, Tex.

J.-B. de Chabalier, Observatoire Volcanologique et Sismologique de Guadeloupe, Le Houëlmont, F-97113 Gourbeyre, Guadeloupe, France. (dechabal@ipgp.fr)

M.-P. Doin and R. Grandin, Laboratoire de Géologie, École Normale Supérieure, CNRS UMR 8538, 24 Rue Lhomond, 75231 Paris CEDEX 05, France. (doin@geologie.ens.fr; grandin@geologie.ens.fr)

E. Jacques, G. C. P. King, and A. Socquet, Institut de Physique du Globe de Paris, Equipe de Tectonique et Mécanique de la Lithosphère, CNRS-UMR 7154, 1 rue Jussieu, F-75238 Paris, France. (jacques@ipgp.fr; king@ipgp.fr; socquet@ipgp.fr)